International Journal of Civil Engineering (2022) 20:151–168
https://doi.org/10.1007/s40999-021-00641-9

RESEARCH PAPER

Experimental and Numerical Study of Seismic Behavior of Shallow Strip Foundation Near Sandy Slope

Sahar Jalili[1] · Hossein Javaheri Koupaei[1] · Hassan Sharafi[2] · Navid Ganjian[1]

Received: 14 February 2021 / Revised: 15 May 2021 / Accepted: 25 May 2021 / Published online: 29 June 2021

Abstract
Placement of shallow foundations near or adjacent to slopes reduces their seismic and static bearing capacities. In this paper, the seismic behavior of shallow foundations adjacent to sandy slopes has been studied using a two-dimensional finite element method. Most of the previous studies have focused on upper bound solutions in limit state analysis framework via pseudo-static loading, and the effects of actual seismic loading such as loading frequency effects, acceleration amplitude above 0.30 g, non-linear dynamic analysis, and so on are ignored. The shallow foundations are located at a certain distance from the slope crest (i.e., d = 0.5b, 1.5b and 2.0b). The slope inclination angle studied in this paper is 25° (1 V: 2 H). The analyzed slope is composed of medium dense sand. The two elastic–perfectly plastic Mohr–Coulomb (MC) and hardening soil (HSM) constitutive models have been considered to investigate the effect of plastic behavior of the sandy soil. Innovatively, the actual seismic behavior of the slope, shallow foundation and the direction of the seismic responses have been studied. The results show that the structural and geotechnical responses of the HSM model are in most cases up to 30% larger and more conservative than the MC model responses. This shows the importance of using the HSM model in the study of seismic stability of slope and foundation.

Keywords Shallow foundation · Dry sandy slope · Seismic loading · Numerical model · Physical model

1 Introduction

The near-slope shallow foundations, form the support of the many engineering structures. By positioning the shallow foundation in or near the slope, its static and seismic (i.e., dynamic) bearing capacities are reduced. This is generally because the *soil confinement conditions* and *wedge failure* formed beneath the shallow foundation in *level* and *sloped* grounds are fundamentally different. The values of the all bearing capacity coefficients that constitute the static or dynamic (seismic) bearing capacity relationships are reduced under these conditions (i.e., slope condition). In fact, as the slope inclination angle increases, the coefficients of the shallow foundation bearing capacity are decreased, correspondingly. Seismic forces can affect the slope and the near-slope footings in the horizontal, vertical, or a combination of these directions. Solving the problem of the horizontal and vertical seismic loading effects is analyzed using the K_h and k_v, the horizontal and the vertical seismic load coefficients, respectively, in the pseudo-static loading technique in the form of the limit equilibrium *(LE)* and limit state analysis *(LSA)* methods. Various analytical, numerical, and experimental studies have shown that generally, the static and seismic bearing capacity of the shallow foundations within or near the soil slopes, decreases in comparison with the level ground condition [1–3]. The problem of the seismic (or static) interaction between the shallow foundation and the soil slope is primarily studied by the limit state analysis or limit

✉ Hassan Sharafi
h_sharafi@razi.ac.ir; Hasansharafi1@gmail.com

Sahar Jalili
saharjalili.c@gmail.com

Hossein Javaheri Koupaei
h-javaheri@srbiau.ac.ir

Navid Ganjian
n.ganjian@srbiau.ac.ir

[1] Department of Civil Engineering, Science and Research Branch, Islamic Azad University, Tehran, Iran

[2] Civil Engineering Department, Engineering Faculty, Razi University, Kermanshah, Iran

equilibrium methods. Most previous studies have used the pseudo-static analysis to solve this problem [2–5]. For example, in some studies, the limit state upper bound solutions have been used to calculate the bearing capacity of the near-slope shallow foundations using Mohr–Coulomb model parameters [2]. The calculation of seismic or static bearing capacity of the within or near-slope foundations (using MC strength parameters) by estimating bearing capacity coefficients such as N_c, N_q and N_γ has been the subject of the most previous studies [6–8]. *Of course, most previous papers, because they have used the limit state analysis (LSA) method to solve the problem of slope and shallow footing seismic interaction, have usually used the Mohr–Coulomb model strength parameters such as c and φ.*

Indeed, various researchers have studied the seismic bearing capacity of the shallow foundations. In their studies, a wide range of main parameters including cohesive soils (clayey soils), granular soils (sandy and gravely soils), strip foundations and quasi-static dynamic loading are assumed. For example, the references [6–9], all have evaluated and studied the seismic bearing capacity of shallow foundations. Another reference paper [10] calculated the seismic bearing capacity factors for the spread foundations. They used the well-known limit state analysis method to extract the seismic bearing capacity factors. Seismic bearing capacity factors are evaluated by many other studies such as [11] (for sloped grounds), [12] (for dry soils), [12] (for footing settlement effects). The reference [13] searched the effect of *slope vicinity* on the seismic bearing capacity of strip footings. Dynamic bearing capacity factors include coefficients for cohesion (N_{cd}), footing static surcharge load (N_{qd}) and soil density ($N_{\gamma d}$) terms in the seismic conditions are often calculated in the framework of the quasi-static method [14–16] using the seismic lateral loading coefficient, K_h.

Seismic bearing capacity factors can be calculated by extending theories related to the extraction of the same coefficients in the static state [17] in terms of inertial and kinematic interaction effects of seismic loads. However, for sandy soils and foundations with zero embedment depth (D_f) (i.e., at ground surface $D_f = 0$, $q = \gamma D_f = 0$), usually only the coefficient N_γ needs to be calculated. For example, the N_γ for rough strip footing using the method of characteristics has been computed [18]. For the problem of adjacent or within earthen slope foundations, the two issues of slope stability and foundation bearing capacity are intricately combined [19]. In this case, the effects of lateral soil movement should be considered in setting the coefficients [20, 21]. The references [22, 23] studies are among the first studies to estimate the bearing capacity of shallow foundations in the presence of slope during static loading. Most of the limit state analysis solutions presented in previous studies have focused on limit state upper bound solutions [24–27] so that the failure loads of the foundation and slope can be obtained with them.

Certainly, the problem of lateral soil movement on sloping ground reduces the bearing capacity of both shallow and deep foundations [28, 29]. In seismic loading cases, the effects of numerical analysis method of simulated models and the directions of seismic loading application can have a great impact on the final responses of the full 3D slope problem [30, 31, 33]. In addition, FELA modeling, which combines the advantages of finite element method and the limit state analysis of plasticity theory, is another method used for seismic analysis of the bearing capacity of shallow foundations [32–34]. Examination of newer researches reveals that the pseudo-static method has been used many times in recent years to calculate the bearing capacity coefficients of shallow foundations during seismic loading [35–37]. Also, physical modeling using shaking table [38] and slip lines method [39] are other common methods of seismic analysis of shallow foundations. In addition, the Newmark sliding block method has been used in valuable studies as an efficient method for seismic stability analysis of slopes [40–43].

However, in most of these investigations, the effects of real seismic loading such as the effects of loading frequency, acceleration amplitude above 0.30 g in time-domain, non-linear dynamic analysis type, changes in static overburden values on the dynamical behavior of the footing and slope, and the soil constitutive model type due to the relative density of sandy soil and many others are ignored. This paper tries to examine some of the mentioned details of these issues.

2 Methodology of the Numerical Modeling

In this research, two-dimensional finite element method is used for numerical modeling. This type of calculations can be performed well by *PLAXIS 2D* software. The shallow foundation is considered as strip footing. Due to the geometry of the sandy slope and the shallow foundation, the *2D plane-strain framework* is used for two-dimensional modeling. In this case, the strains perpendicular to the 2D modeling plane are negligible. The strip foundation is made of reinforced concrete with linear-elastic mechanical behavior. In fact, the foundation concrete does not enter to the plastic region (or plastic strains) during seismic deformations but the soil enters the plastic phase. Reinforced concrete strip footing dimensions are 1 m thick (t = 1.0 m) and 2 m wide (b = 2.0 m).

2.1 Details of the Model's Geometry

The distance of the outer edge of the shallow foundation to the edge of the slope crest (d) is selected as a variable and includes d = 0.5b, 1.5b and 2.0b. In fact, the distance of the shallow foundation edge varies relative to the slope crest. The linear-elastic modulus of the reinforced concrete (i.e., RC) is assumed to have a common value equal to $E_{RC} = 25GPa$ and its *Poisson's ratio* is $v = 0.15$ for high strength concrete. The specific gravity of the reinforced concrete is $\gamma_{RC} = 25kN/m^3$ (in terms of the effect of bar reinforcement on the shallow foundation weight). The Mohr–Coulomb (MC) elastic–perfectly plastic criterion under the non-associated plastic flow rule (i.e., assuming zero dilation angle for sand) was used for modeling the dry sandy soil. The relative density of the dry sandy slope is moderate and the soil grain size is fine. The relative density of this kind of fine sand is quantitatively in the range of 50–60%.

The sand soil parameters obtained from the shear strength tests are presented in Table 1. Fine meshing is used to create the finite element meshes to pass the generated seismic waves properly. The effect of finite element meshing on seismic results has been measured using very small and medium size meshes. To analyze the sensitivity of mesh, three densities of FE meshes, including the medium, fine and very fine meshes have been used, and finally the observed difference in responses has been less than 4%. Subsequently, the very fine mesh density is selected. It should be noted that *15-node triangular elements* are used to mesh the 2-dimensional (2D) finite element models. These types of triangular meshes are well compatible with 2D plane-strain modeling logic. All calculations in this study can be performed well by a commercial finite element software such as *PLAXIS 2D*. The dry sandy slope is statically stable and its stability *safety factor* (FS) is greater than one. As the height of the sand slope increases, its static stability and then its seismic stability decreases. Higher slopes are always more prone to rupture and slipping than shorter slopes. In high soil slopes, rupture can be local or general. Slope rupture and instability, locally or in general, can reduce effective stresses under the adjacent slope foundation. By reducing in situ stresses and reducing the amount of soil confinement under the foundation, its bearing capacity is reduced. Increasing the angle of the earth slope also reduces its stability due to the instability of the materials forming the body of the slope. As the slope angle increases, the slope grains material is more likely to slip on top of each other, which causes the soil to move laterally below the surface footing. The removal or lateral displacement of sandy soil particles from the shallow foundation reduces its bearing capacity due to the reduction of confining stresses.

In fact, instability of the slope and shallow foundation near the crest of the slope occurs during the seismic loading. The rigid interface between the reinforced concrete footing and the sandy soil has been considered. In fact, due to the high rigidity of reinforced concrete foundations, the initial assumption of a rigid interface is used. Due to the parametric nature of the seismic studies of the present paper and in terms of various parameters, a more detailed study of the stiffness of the interface location has been omitted and the value of R in the interface section of reinforced concrete–sandy soil interface has been assumed to be one (R = 1.0). In principle, the assumption of a rigid interface between reinforced concrete foundation and dry sandy soil is assumed to be the same in all the performed numerical analyzes.

In Table 1, it must be noted that the unloading–reloading elastic modulus is equal to three times of the *oedometric* (or tangent) elastic modulus (i.e., $E_{ur} = 3.0E_{oed}$) and secant elastic modulus is equal to 1.25 times of the tangent elastic modulus ($E_{50} = 1.25E_{oed}$). Moreover, the strength parameters of sandy soil including the *peak friction angle,* φ_{pk}

Table 1 Introducing the parameters used to define the two MC and HSM constitutive models for the dry sandy slope materials

Sandy soil parameters	MC model symbols (unit)	HSM model symbols (unit)	Values
Angle of internal friction of the soil	(Degree)φ	$_{pk}$ (Degree)φ	32.00
Soil cohesion	C (kPa)	C (kPa)	0.00
Elastic modulus of soil	E (MPa)	E_{50} (MPa)	42.50
Poisson's ratio of soil	V	V	0.20
Dilatation angle of soil	ψ (Degree)	ψ (Degree)	0.00
Specific gravity of dry sandy soil	γ (kN/m^3)	γ (kN/m^3)	16.00
Elastic modulus of tangent or odometer	–	E_{oe} (MPa)	34.00
Elastic loading–unloading modulus	–	E_{ur} (MPa)	102.00
The coefficient of earth pressure at rest, K_0	–	K_0	0.47
Hardening dependency on stress level coefficient	–	M	0.50

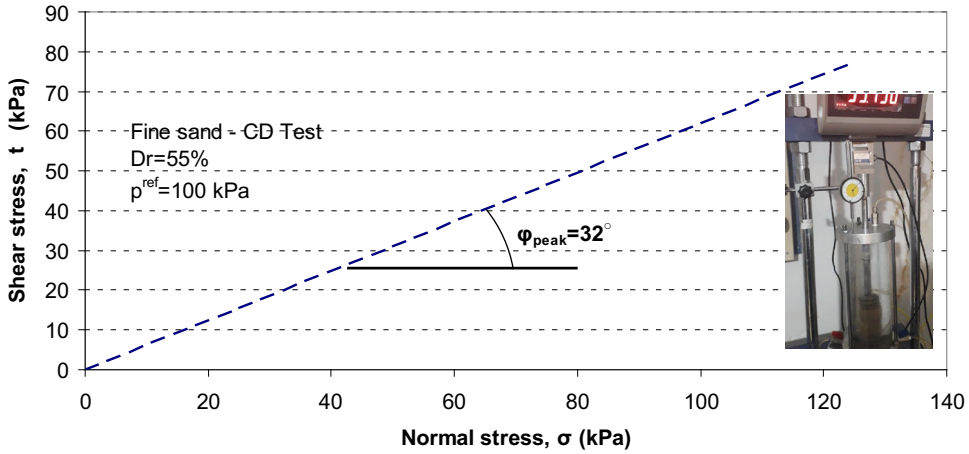

Fig. 1 Results of the consolidated-drained triaxial test (CD test) on the fine sand for soil sample with 55% relative density

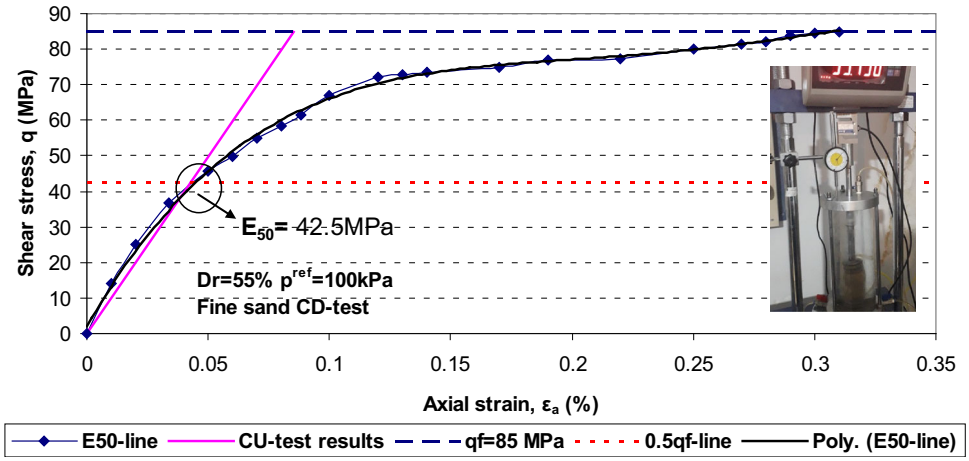

Fig. 2 Results of the consolidated-drained triaxial test (CD test) on the fine sand for soil sample with 55% relative density

and *cohesion, c* are derived from consolidated-drained triaxial test on the soil samples under different overburden conditions (Fig. 1). Furthermore, the sandy soil stiffness parameters including the secant elastic modulus (i.e., E_{50}) is extracted from the consolidated-drained triaxial tests (i.e., CD tests) for different depths (i.e., different soil surcharge stresses). However, the reference values for the strength parameters (including C^{ref}, φ^{ref}) and the stiffness parameters (including E^{ref}_{50}) all are considered in a reference mean pressure of 100 kPa (i.e., p^{ref} = 100 kPa, see Fig. 2). In Table 1, note that all the parameters required to define the two constitutive models of MC and HSS have been obtained by performing shear strength tests on fine sandy soil. In these experiments, the relative density of sandy soil and the reference pressure (i.e., p^{ref}) applied are considered as two key factors. Also in Table 1, *m-power* parameter is approximately 0.5 for granular soils and about one for cohesive soils. Parameter m shows the dependence of soil stiffness on the stress level and soil strength parameters. The m-power achieves a non-linear and hyperbolic relationship between stiffness and stress level in soil. In cohesive soils, such as clay, stiffness is generally not a non-linear function of stress level, but in granular soil, stiffness is a function of confinement and overhead stresses. Also, the coefficient of earth pressure at rest, K_0 is assumed to be equal to $K_0 = 1-\sin\varphi_{pk}$. On the other hand, due to the fine-grained sandy soil and its low relative density, the assumption that the dilation angle is close to zero is largely true. Table 2 presents the yield (i.e., *f-function)* functions of the Mohr–Coulomb (MC) and hardening soil (HSM) constitutive models. It should be noted that the yield functions of these models as well as the yield cap of the HSM model are provided in the *p'-q stress* space.

Figure 3 illustrates the geometry of the whole model under study. The *reference point A* is right on the edge of the slope crest as a key point in recording the time-history responses in subsequent sections of the paper. As shown in

Table 2 Yield functions/surfaces of the used two soil constitutive models

Constitutive models	Yield or plastic potential function (f or g, respectively)
Mohr–Coulomb (MC) *(θ is the Lode's angle)*	$f = \left(\sqrt{3}cos\theta - sin\theta sin\varphi\right)q - 3'psin\varphi - 3ccos\varphi = 0$
Hardening soil model (HSM) *(α and β are the cap parameters, γ_p is the plastic hardening parameter)*	$f = \overline{f} - \gamma^p$ $\overline{f} = \frac{2}{E_i}\frac{q}{1-\frac{q}{q_a}} - \frac{2q}{E_{ur}}$ *Cap yield surface:* $f^c = \frac{q^2}{\alpha^2} + {}'p^2 - p_p^2$ $\delta = (3 + sin\varphi)/(3 - sin\varphi)$ $\gamma^p = -\left(2\varepsilon_1^p - \varepsilon_v^p\right) \approx -2\varepsilon_1^p$ $\varepsilon_1^p \approx \frac{1}{2}\overline{f} = \frac{1}{E_i}\frac{q}{1-q/q_a} - \frac{q}{E_{ur}}$ $q = {}'\sigma_1 - {}'\sigma_3$ $'p = -({}'\sigma_1 + {}'\sigma_2 + {}'\sigma_3)/3$ $\tilde{q} = {}'\sigma_1 + (\delta - 1){}'\sigma_2 - \delta'\sigma_3$ $\varepsilon_v^{pc} = (\frac{\beta}{1-m})\left(\frac{p_p}{p^{ref}}\right)^{1-m}$

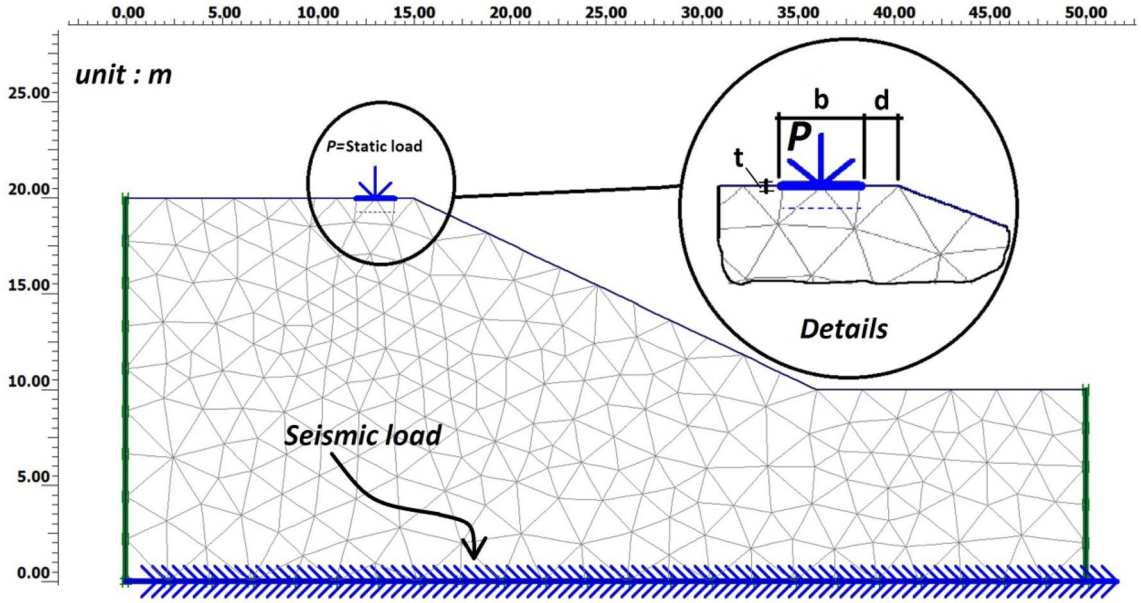

Fig. 3 Geometry and static-seismic boundary and initial conditions (Fine mesh case)

Fig. 3, the shallow foundation with width b is located at the distance d from the crest of a dry sandy slope. Due to the parametric nature of the numerical modeling of the present study and addressing other important variables such as static surcharge load variations and the type of the soil constitutive model, the *setback distance d* in all of the study was varied as 0.5b, 1.5b and 2.0b. According to Fig. 3, the seismic load is applied as the acceleration time-history record of Tabas near-field earthquake in the bedrock of the slope numerical model in the lowest height level.

Numerical modeling of the problem is performed in three distinct and successive phases. In the first phase, the static model of the slope is defined and executed. In the second phase, the in situ static condition of the slope model, shallow foundation, and a static vertical surcharge load are produced. In the third phase, the dynamic loading is applied to the final stabled model of the second phase. The static boundary conditions in the static phases include the roller support on the left and right sides of the numerical model and the fixed support on the bottom level of the numerical model. Dynamic boundary conditions in the third phase of numerical modeling include the *adsorbent boundaries* on the walls and the bottom of the numerical model. *Absorbent boundaries* have been applied to the 2D finite element model to prevent the return of seismic waves into the numerical model. The return of seismic waves into the numerical model cause some *unwanted errors* in the final analysis results.

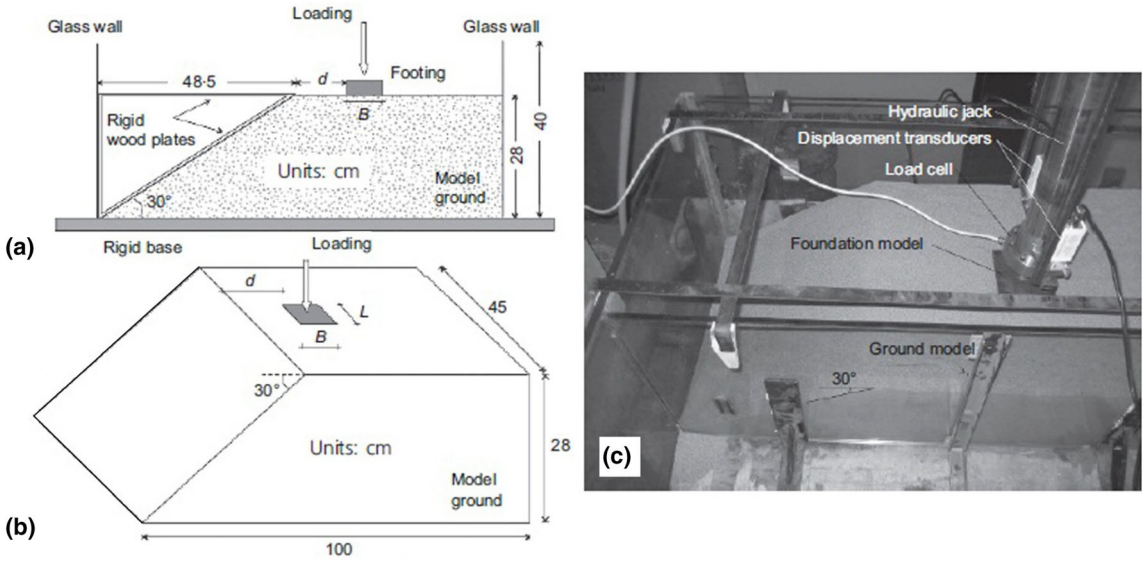

Fig. 4 Schematic and real form of the experimental model of Castelli and Lentini's (2012) study [1], including: **a** 2D geometry, **b** 3D shape, and **c** real image of dry sandy slope model

2.2 Verification of Numerical Modeling

2.2.1 Verification of the Numerical Modeling in the Static Step

The closest existing study to the subject of this research has been used to validate the results of the static step of the numerical modeling of the present paper. Accordingly, the results of the experimental study performed by reference [1] are used. According to Fig. 4, a 30° sandy slope forms the experimental model for this study. Dry sand with a relative density of 78% and an internal friction angle of 38° is placed into a physical modeling box, layer by layer. The maximum specific gravity of sandy soil was measured as 17.5 kN/m^3. Two square and strip footing models have been used in reference [1] study, to approximate the numerical results of the present paper, the diagrams of the output of the plane-strain model of the strip footing physical model is used to get closer to the numerical models. Strip foundation model in reference [1] were made of rough surface steel plates. All the experiments were performed on dry sandy slope samples made from Playa Catania sand collected from Italy. The width of the strip foundations B is equal to 4 cm. Sandpapers are attached to the bottom of the steel shallow foundation model to provide the sufficient friction between the footing physical model base and the dry sandy soil. The numerical modeling of a number of physical models of this study is implemented to validate the numerical results of the present study. During the validation process, the linear-elastic criterion was used to model the steel plate shallow foundation model and the soil behavior has been simulated

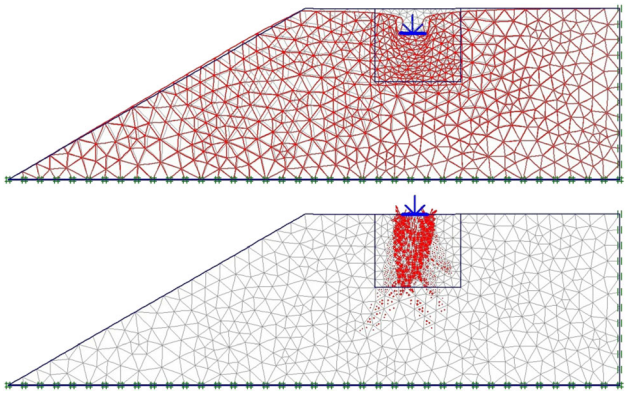

Fig. 5 Results of deformation and distribution of shear strains for the validation model with steel footing dimensions $B = 4$ cm and distance $d = 16$ cm

using the *Mohr–Coulomb* (MC) model. *It should be noted that the process of simulating the physical model of a strip foundation relied on a sandy slope is fully consistent with the two-dimensional assumptions of the plane-strain models.*

Figure 5 is an example of a numerical model, created to validate the present paper static step model results. Figure 6 shows the results of the deformation and shear strain distribution for the validation model with strip footing dimensions $B = 4$ cm and distance $d = 16$ cm. Three adjacent distances equal to 16, 30 and greater than 30 cm are considered for parameter d. According to Fig. 6, the load–settlement curve derived from the validation of the reference paper's [1] experimental model is simultaneously shown by the results of the numerical modeling of the present paper. As shown in Fig. 6, there is a good

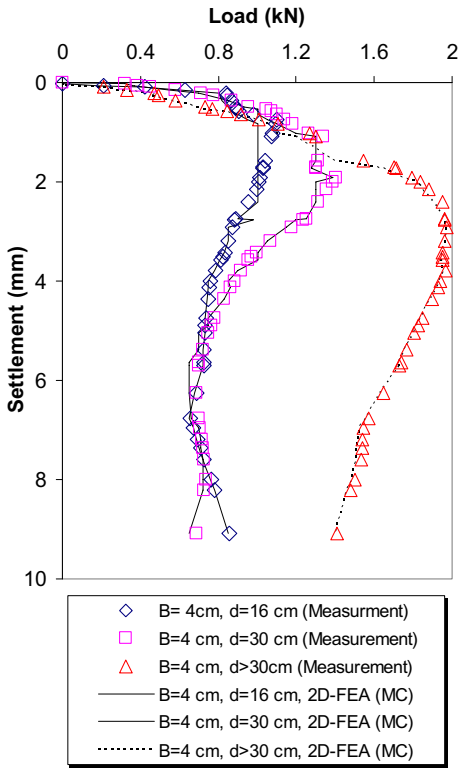

Fig. 6 Load–settlement curve derived from the validation of the selected reference paper [1] experimental model test results

agreement between the experimental results obtained by the reference paper [1] and the 2D-FEA numerical findings of the present study for the strip footing model.

2.2.2 Verification of the Numerical Modeling in the Dynamic Step

The results of the horizontal and vertical deformations of a seismic model have been used to verify the numerical models of the research as well as the software and selected numerical method of the present study (*in the seismic loading phase)*. For this purpose, a model similar to and close to the numerical model of the present study was presented in the reference paper of Ausilio and Zimmaro (2015) [35] in which a seismic design of a shallow foundation with a width of 2.0 m located at the edge of the rock slope by the elasto-plastic Hoek–Brown constitutive model with the parameters similar to the Mohr–Coulomb model is considered and used. The seismic loading of this model includes the record of the Northridge earthquake in 1994 (at *Griffith Park station*) with a duration of about 45 s (Fig. 7b). The maximum acceleration of this earthquake is measured for seismic load equal to $PGA = 0.289\ g$. Also, the selected slope is a 45.0° rock slope with a shallow foundation located right at its crest edge. More complete specifications of this model are given in the selected reference article [35]. The diagram of the horizontal and vertical deformations of the point *M* (Fig. 7a) in the model of this slope [35] is extracted and plotted in terms of seismic loading time (second unit) and displacements (centimeter units). However, the specific unit weight of the rock materials is equal to 20 kN/m^3. The linear static surcharge load is set at 8200 kN/m.

Figure 8 displays a relatively good agreement between the results of the selected reference paper model displacements [35] and the two-dimensional finite element modeling findings (2D-FEA) of the present study. On the

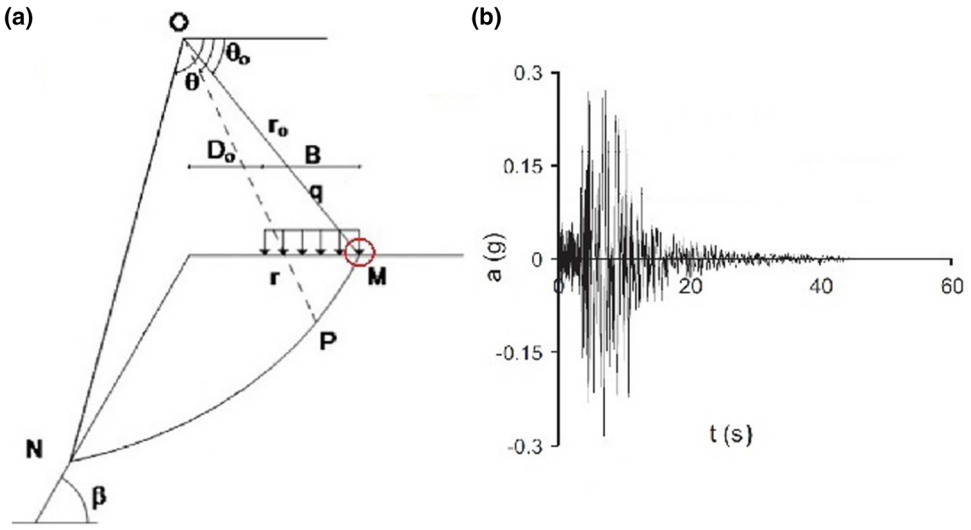

Fig. 7 Details of reference model of the reference [35] analyzed in the dynamic step verification: **a** problem's geometry, **b** Northridge earthquake input motion

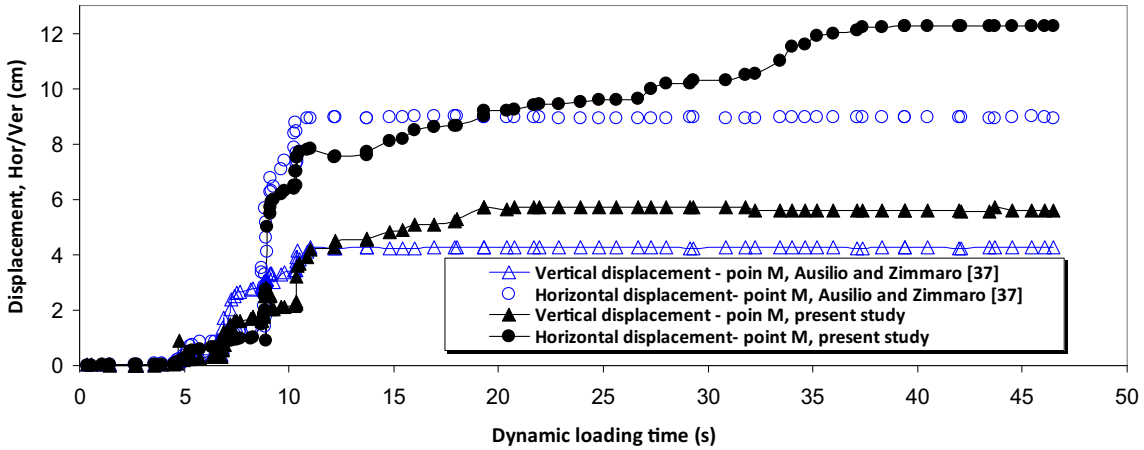

Fig. 8 Comparison of the verification results of the reference article model [35] and the finite element model implemented in the present study

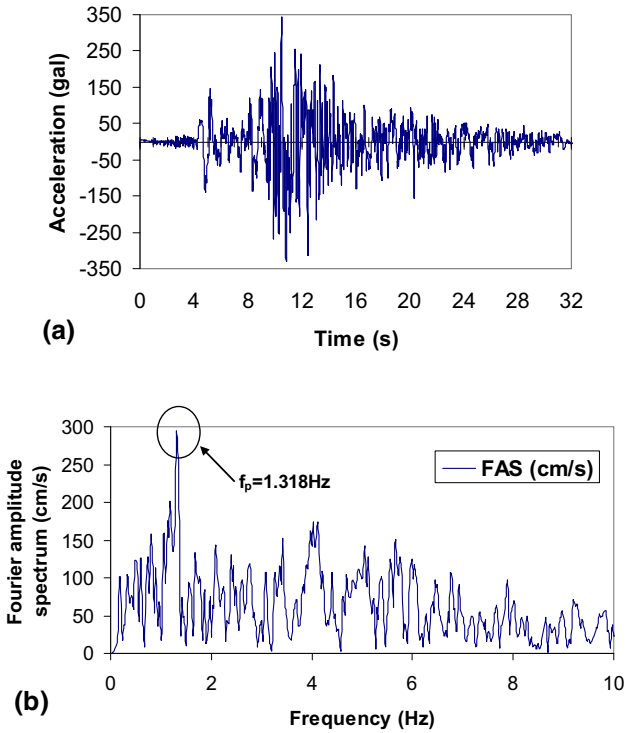

Fig. 9 Time-history and frequency distribution (FAS) graphs of the used input motion: **a** acceleration time-history, **b** Fourier amplitude spectrum (FAS)

other hand, the difference in the results can be due to the FE meshing effects as well as the static and dynamic boundary conditions of the numerical modeling.

2.3 Input Seismic Motion Details

In most previous papers related to this topic [6–12], *pseudo-static simplified loading* has been used and the horizontal seismic load factor (K_h) is typically considered less than 0.30, in the range of 0.1–0.25. In this study, both the real seismic loading and the non-linear dynamic time-history analyses are applied. Accordingly, based on Fig. 9a, the longitudinal component record of the Tabas earthquake is scaled to 0.35 g (i.e., acceleration amplitude) at the near-fault station of Tabas. The Fourier amplitude spectrum (FAS) of this earthquake record can be seen in Fig. 9b. According to Fig. 9b, the predominant frequency of the Tabas earthquake is generally between 1 and 1.5 Hz. As can be seen in Fig. 9a, the earthquake record time duration is about 33 s. The main purpose of this study is not to focus on the *frequency behavior* (i.e., *f values*) or seismic loading predominant period (T*p*) and only to compare the time-history behavior of the two different constitutive models for the shallow foundation-sandy slope problem. But on the other hand, the seismic loading input has been selected in such a way that it has the ability to create non-linear and plastic deformations in the sandy slope and even in the reinforced concrete (RC) foundation.

3 The outputs of Numerical Modeling

The expansion/development of the plastic strain zones around and below the shallow foundation and on the slope oblique body can provide useful information on the static and seismic behavior of the shallow foundation-slope set. Therefore, Fig. 10 shows how the shear strain zones extend around the shallow foundation (for most critical distance case d = 0.5b) and on the slope with increasing the static surcharge load.

3.1 Extension of the Plastic Zones Below the Foundation and on the Slope

The contours shown in Fig. 10 are the results of the Mohr–Coulomb model static pre-analysis phase *and just before*

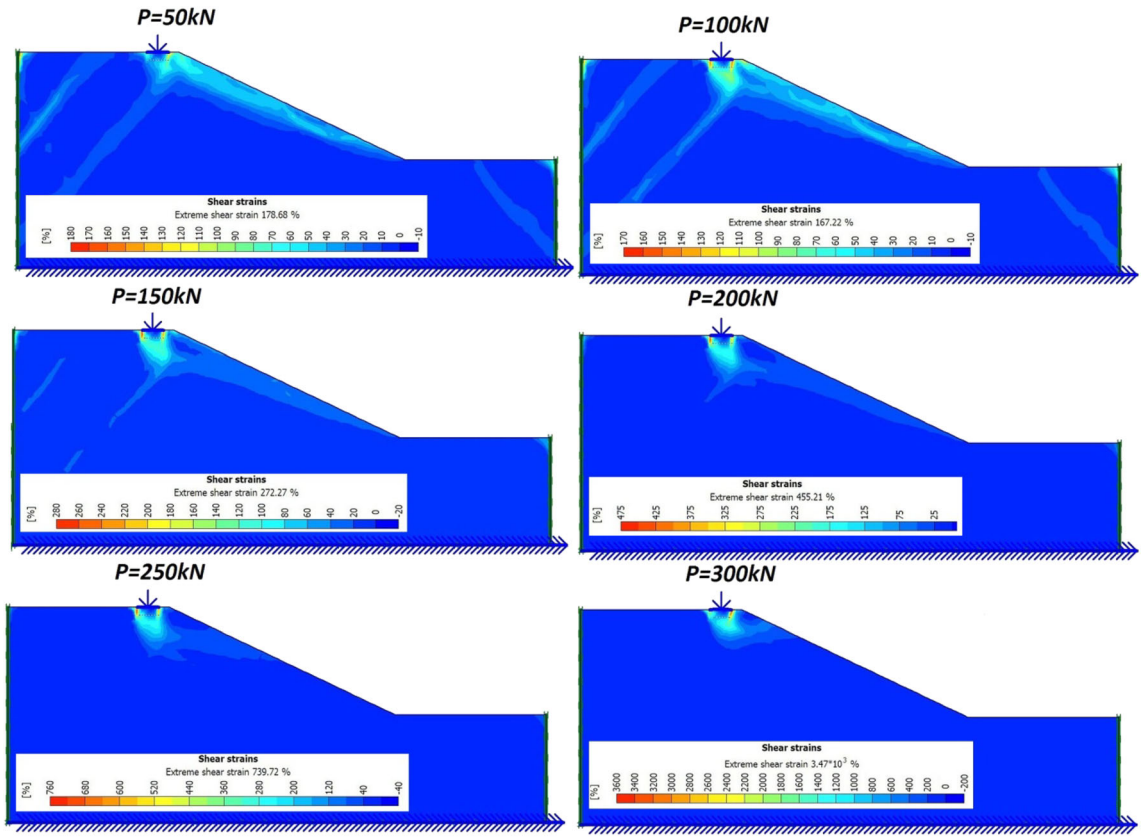

Fig. 10 The development of the shear strain zones around the shallow foundation and on the slope with increasing the static surcharge load (*for case: d = 0.5b*)

the seismic loading. According to Fig. 10, with increasing the static surcharge load, the maximum shear strain zone is shifted from the slope surface to under the shallow foundation with higher/concentrated shear strains. The main reason for this is that the concentration and amount of shear strains are transferred from the surface area of the slope to the beneath of the shallow foundation by increasing the static surcharge load. It is true that at lower surcharges, the sloping part also has a shear strain distribution, but its values are much lower. In fact, not only the pattern of shear strain propagation on the slope is important, but also the quantitative values of each strain expansion/development pattern below the footing and in the oblique body of the slope are also very important. Indeed, with increasing the static surcharge loads, the actual shape of the soil failure beneath the shallow foundation is better displayed.

Figure 11 illustrates how the plastic zones extend around the shallow foundation and on the slope with increasing the overburden. Accordingly, with the increase of the static surcharge load, the triangular wedge beneath the surface of the strip shallow foundation is further expanded and more points of that become plastic. According to Fig. 11, in all cases, three concentric triangular wedges are formed beneath the shallow foundation. The first (i.e., the smallest wedge) triangular wedge is formed just below the strip shallow foundation. The second wedge (i.e., the medium-sized wedge) is formed in the perimeter of the first wedge and the third wedge (i.e., the largest wedge) is in the second wedge perimeter. In addition to the wedges beneath the shallow foundation, as shown in Fig. 11, more points on the slope surface experience plastic yielding by increasing the static surcharge load.

Figure 12 shows the extension of plastic zones around the shallowoundation and on the slope with increasing the surcharge load in the HSM. s shown in Fig. 12, most of the sloping part of the numerical model undergoes plastic hardening. Some points of the slope with plastic hardening are marked with *green-colored* squares. The Mohr–Coulomb model elastic-perfect plastic zones under the shallow foundation (i.e., red-colored hollow squares) are also expanded further with increasing the static surcharge load under the shallow foundation zone.

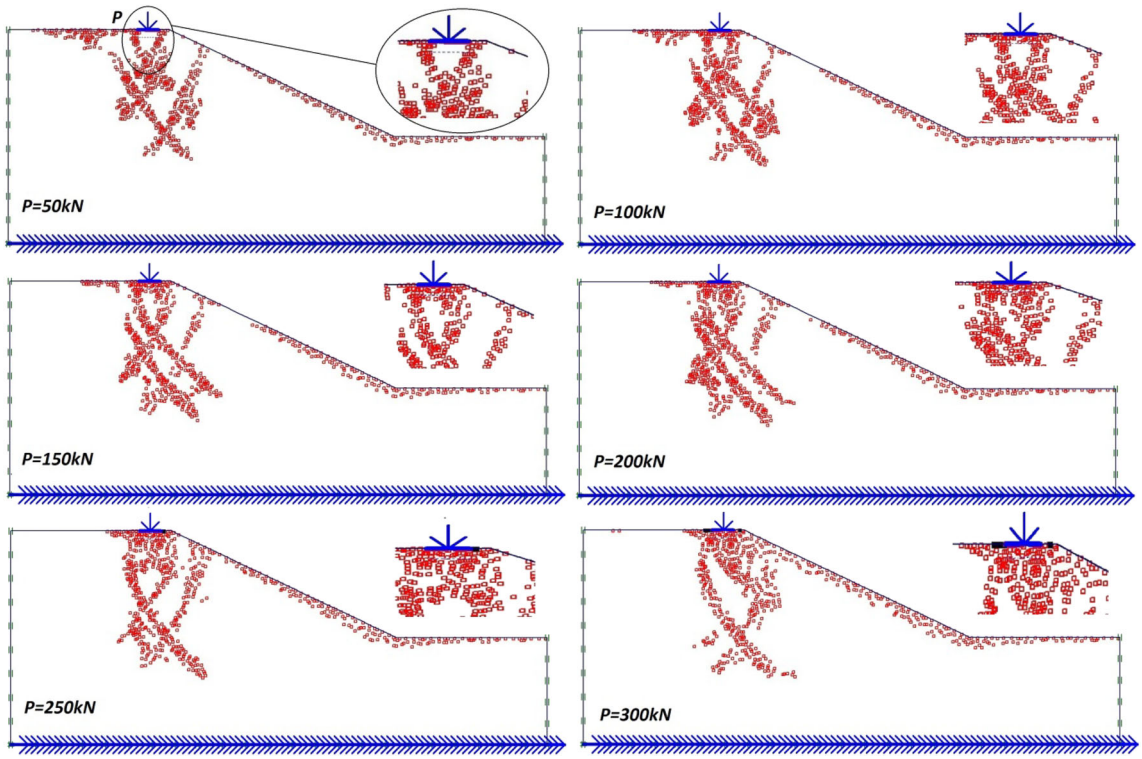

Fig. 11 Extension of the plastic zones around the shallow foundation and on the slope with increasing the static surcharge load (for case: $d = 0.5b$)

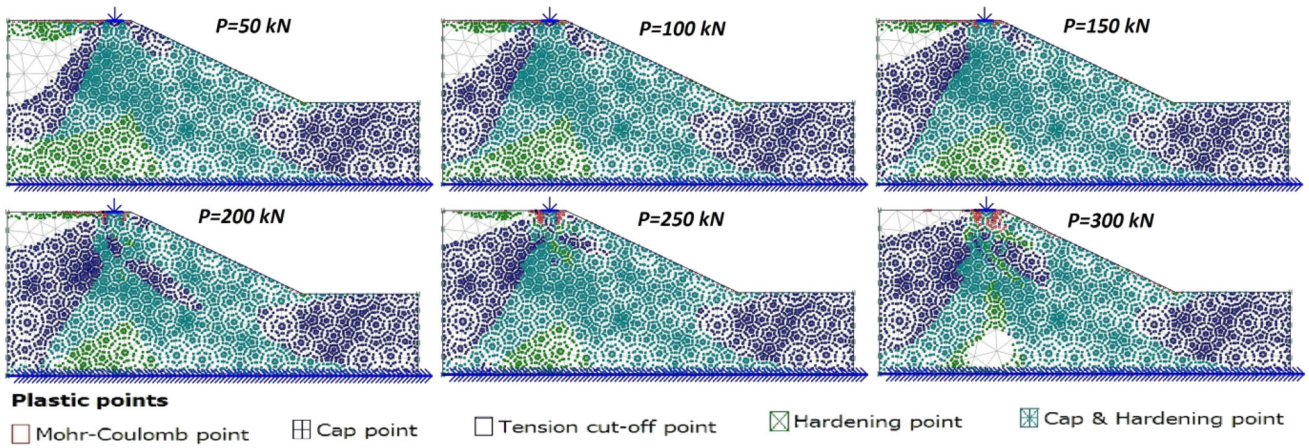

Fig. 12 Extension of the plastic zones around the shallow foundation and on the slope with increasing the surcharge load in the HSM (for case: $d = 0.5b$)

3.2 The Structural Behavior of the RC Strip Foundations in Terms of Load-Deformation

To investigate the load-deformation behavior of the shallow foundation, the structural outputs are considered. Structural outputs mainly include bending moments, axial and shear forces. Moreover, the deformation and shear strain under the shallow foundation illustrate the *interactive behavior* of the shallow foundation and slope. The value of the *setback distance d* in these diagrams is variable according to the width of foundation, b and is equal to the distances of 0.5b, 1.5b and 2.0b, respectively. The following figures (i.e., Figs. 13–18) have been used for comparing the MC and HSM constitutive models results. According to the engineering judgment, these internal effort parameters are variable during the seismic loading time per second and the purpose of their presentation was to compare the differences for the two constitutive models

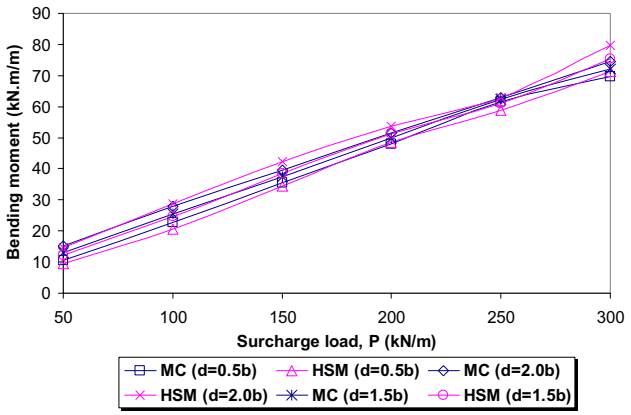

Fig. 13 Changes in dynamic bending moments produced in the foundation for the static surcharge load changes

MC and HSM without and with the assumption of strain hardening, respectively. Regarding sandy soils with low-to-medium relative density, the problem of strain hardening and *contraction shear* can have significant effects on the final results. In the findings of this paper, this difference between the results of the two constitutive models is evident. In fact, none of the results show relative or complete compliance.

Figure 13 reveals how the dynamic bending moment produced in the foundation changes as the static surcharge load changes. Accordingly, the MC model bending moment is slightly higher in most static surcharge loads for small *setback distances d* than the bending moment created by the HSM model. Due to hardening strains, more seismic energy reaches the soil and the foundation, therefore, the internal efforts such as bending moment is reduced. According to Fig. 13, with increasing the static surcharge load, the dynamic bending moment in the foundation increases with an upward trend. According to this diagram, with increasing the distance *d* of the foundation from the edge of the slope's crest, a small amount of bending moment in the foundation has increased. The reason for

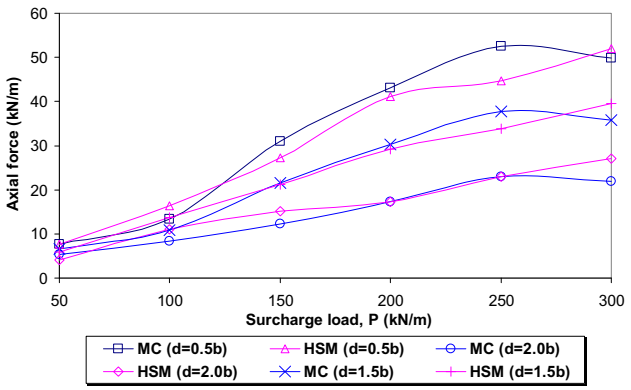

Fig. 14 Dynamic axial force changes produced in the foundation for the static surcharge load changes

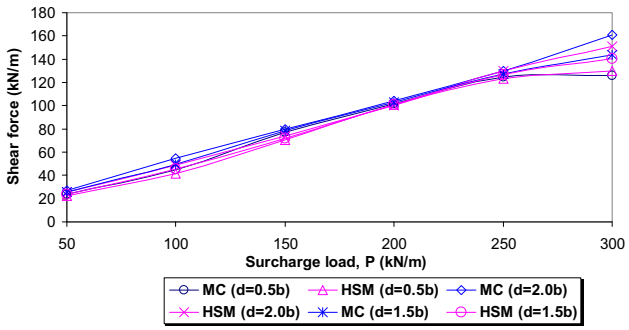

Fig. 15 Dynamic shear force changes produced in the foundation for the static surcharge load changes

this is that by increasing the distance of the foundation from the slope crest, more amounts of stress are transferred to the reinforced concrete body of the foundation, because the deformation of the slope neutralizes and dissipates greater part of the forces on the shallow foundation. In interpreting Fig. 13 in relation to the following Figs. 14 and 15, due to the effect of the direction of seismic wave propagation in comparison to the *directions* of the axial force, shear force and bending moment, sufficient attention should be paid.

Figure 14 shows the dynamic axial force changes produced in the shallow foundation for static surcharge load changes and Fig. 14 indicates the dynamic shear force changes produced in the footing for the static surcharge load changes. According to Figs. 14 and 15, the behavior of axial and shear forces in the shallow foundation is not similar to that of the bending moment in comparison with the previous diagrams in Fig. 13. The axial and shear forces obtained by the MC constitutive model are slightly higher than the HSM model. However, the reason of which is similar to the cases reported for the bending moment in previous Fig. 13. According to Figs. 14 and 15, with the increase of static surcharge load, the dynamic axial and shear forces of the rigid foundation increase with an ascending trend. As shown in Fig. 14, with increasing the distance from the slope crest, the dynamic axial force in the foundation decreases due to the reduction of the effect of unbalanced slope lateral stresses on the foundation and its internal forces.

According to Fig. 15, with increasing the distance of the foundation from the crest of the slope, the shear force in the foundation has almost increased. The main reason for this is in the direction of shear forces, which by moving away from the slope crest, the shear reaction reaches the shallow foundation more, and the main direction of seismic loading and creating shear stresses is also produced in the same direction of shear forces. However, in interpreting the shapes of this section figures, we must pay attention to the difference between the direction of axial and shear forces

generated in the foundation compared to the direction of propagation of the earthquake shear waves. Basically, the nature and direction of the axial and shear forces in the foundation as well as the seismic bending moment in it are completely different, therefore, the diagrams have created contradictory trends and patterns.

Figure 16 displays the changes in the static horizontal (lateral) displacements produced in the slope in return to the static surcharge load changes for two different constitutive models. The content presented in explaining previous Figs. 13, 14, 15 is realized in diagrams shown in present Figs. 16, 17, 18. So that, in the all cases, the deformation and shear strains produced by the HSM model, are larger than the conventional MC model responses. In fact, the seismic behavior and the responses of the two MC and HSM constitutive models are quite different in previous Figs. 13, 14, 15 and present Figs. 16, 17, 18 and exactly the opposite of each other, respectively. Figure 17 shows the vertical static displacement (i.e., settlement) produced in the foundation versus the static surcharge load changes and Fig. 18 shows the changes of static shear strains produced under the foundation against the static surcharge load changes. The justification for this will be in line with what has been said before. In fact, the possibility of more deformation and strain occurs that prevents from the accumulation of seismic forces in the shallow foundation and creates less internal effort. The occurrence of displacements and strains with an increasing trend helps to unloading as much as possible from the foundation. The occurrence of this seismic *unloading* has led to a reduction in the amount of internal effort in the foundation, including bending moment, axial force and shear force in the previous figures (see previous Figs. 13, 14, 15).

3.3 Seismic Behavior of Sandy Slope Crest

In this section, the behavior of the acceleration responses and the seismic displacements of the elastic–perfectly plastic Mohr–Coulomb (MC) and hardening soil (HSM) constitutive models are compared (for case d = 0.5b). The vertical static surcharge load variations are also considered to have a better comparison between the results. For this purpose, three different surcharge loads of 50, 200 and 300 kN are considered to extract the outputs of this section. Figure 19 compares the horizontal and vertical acceleration time-history responses of the two MC and HSM constitutive models for different static surcharge loads *in most critical case with d = 0.5b*. According to different parts of this figure, the response of the HSM is larger than that of the MC model. The *main reason* for this is the occurrence of plastic strain hardening in the HSM model compared to the MC model. In addition, the dry sandy slope undergoes *geometric hardening* (i.e., decreasing the inclination angle of the slope) during seismic loading. Therefore, estimating the behavior of the soil slope seismic model by a model involving the soil strain hardening will be more accurate.

Figure 20 shows the frequency response diagrams including the Fourier amplitude spectrum for horizontal accelerations (left column) and vertical accelerations (right column) of previous Fig. 19 according to the change in the soil constitutive model and the amount of static surcharge load on the shallow foundation. According to this figure and similar to the time-history response of accelerations in the previous Fig. 19, the hardening soil constitutive model also gives larger frequency response amplitude. The reason for this is basically because the acceleration responses of the HSM model in the time-domain are larger than the acceleration responses of the MC model, so the frequency amplitude responses are also larger. In fact, the amplitude of responses of the time-domain and the frequency-domain are directly related. Also, according to Fig. 20, the amplitude of the vertical acceleration responses (i.e., a_y) is greater than the amplitude of the horizontal acceleration responses (i.e., a_x). The main cause of magnification in the vertical acceleration response (a_y) is due to its direction and its alignment with the direction of static surcharge loading on the shallow footing.

Figure 21 compares the horizontal and vertical displacement time-history responses of the two MC and HSM constitutive models for different static overburdens in most critical case d = 0.5b. By comparing the two right and left columns in these figures, it becomes clear that the hardening soil model (i.e., HSM) always exhibits larger horizontal and vertical deformation responses than the *elastic–perfectly plastic* MC model. *The reason is that the HSM model's strain range enters the strain hardening phase* and causes larger deformations; however, the MC model does not have such strain ranges during seismic loading occurrence. According to sections (a)–(f) of Fig. 21, the occurrence of strain hardening has increased the values of the soil slope permanent plastic displacement responses.

4 Summary and Conclusion

In this study, the real dynamic behavior of the shallow foundation was constructed on dry sandy slope is studied, innovatively. Numerical and experimental modeling results were used to perform the present study and to validate its findings. The plane-strain 2D finite element models of the strip footing are created near the slope crest. The depth of *foundation embedment* is assumed to be zero (i.e., footing on the soil surface) and just above the ground. Two soil constitutive models include the MC and the HSM models have been considered for modeling the dry sandy slope

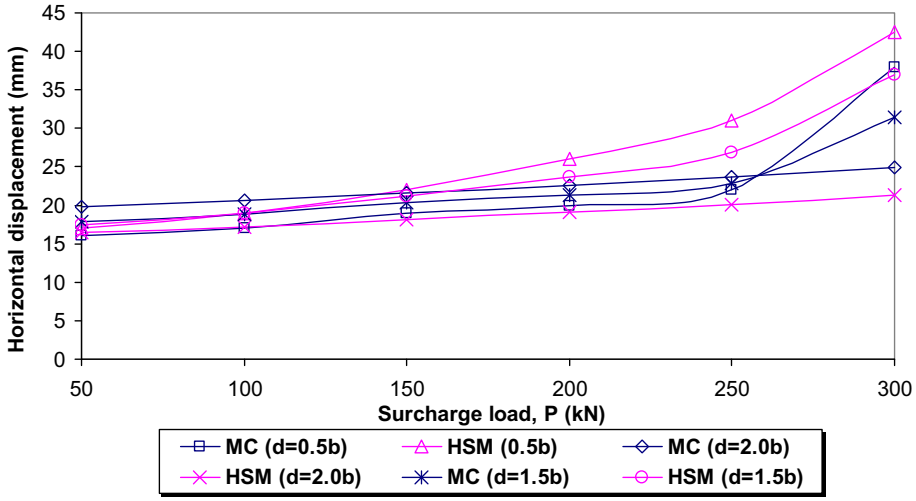

Fig. 16 Changes in the static lateral displacements generated in the slope against the static surcharge load changes

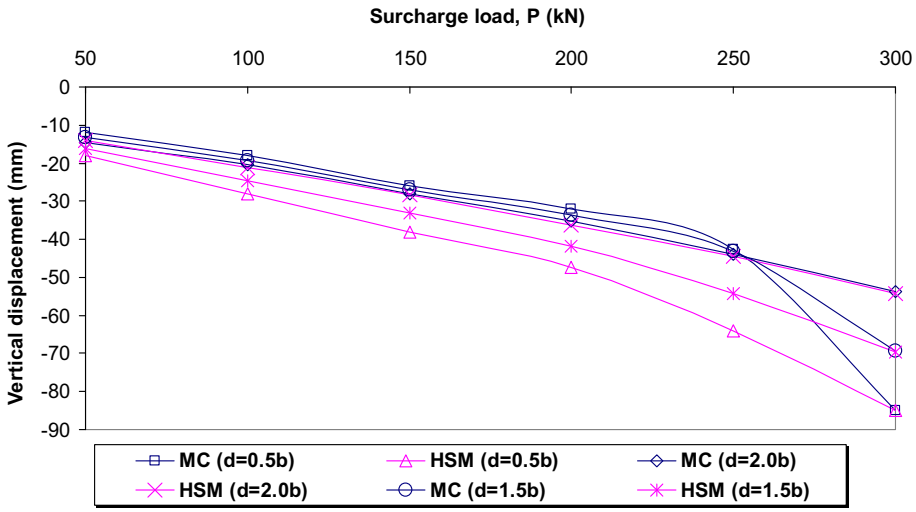

Fig. 17 Changes in the static vertical displacements (settlement) produced in the slope versus the static surcharge load changes

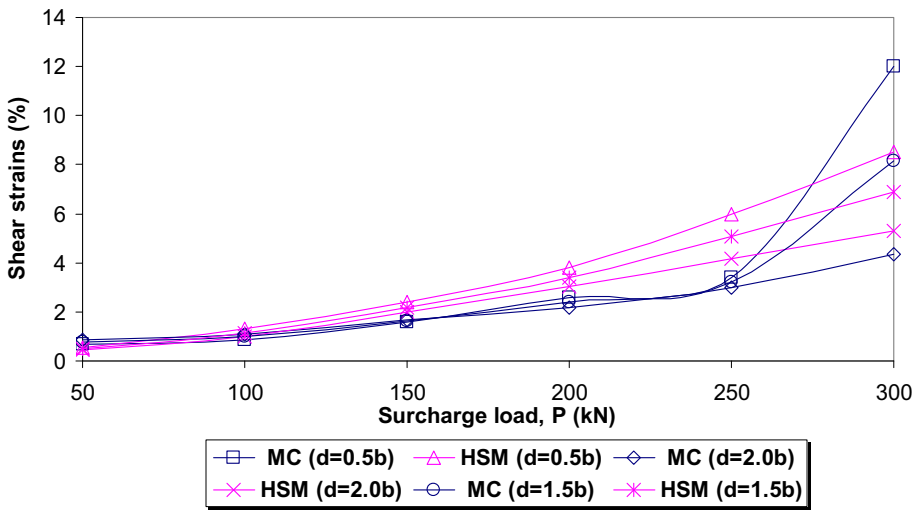

Fig. 18 Changes in the static shear strains produced below the foundation against the static surcharge load changes

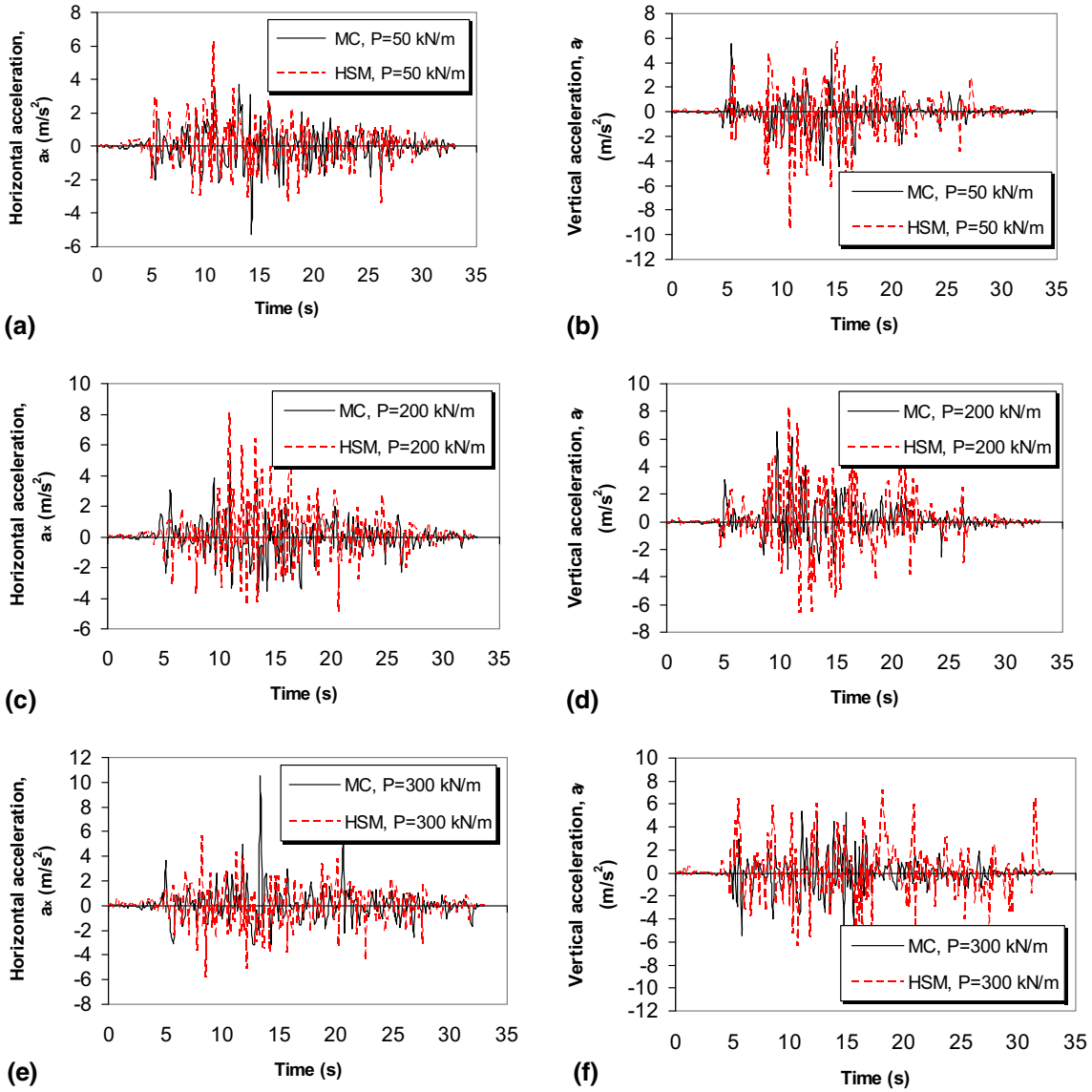

Fig. 19 Comparison of the horizontal and vertical acceleration time-history responses of two MC and HSM models for different static surcharge loads (for $d = 0.5b$ case)

with static surcharge load changes of the strip foundation under *50 kN* load steps. The ranges of internal efforts of the shallow foundation (including axial forces, shear forces, bending moments and etc.) and the horizontal and vertical displacements of the slope and foundation are the main parts of the practical findings of the present paper applicability. Changes in these parameters have been evaluated for two widely used soil constitutive models, MC and HSM, and the degree of difference in the responses has been objectively determined. For accurate seismic design of a shallow foundation adjacent to a slope, it is necessary to determine the amount of internal effort such as bending moments and shear forces that have been considered in this research. The overall results of the numerical studies of this paper are as follows:

1- With the increase of static surcharge load, the shear strain zone shifts from the slope oblique surface to beneath of the shallow foundation and it is concentrated there.

2- In most of the steep part of the slope numerical model the plastic hardening area has been developed. The elastic–perfectly plastic Mohr–Coulomb (MC) zone under the shallow foundation (i.e., the red-colored hollow squares) has also expanded further under the foundation with increasing the static surcharge load.

3- The response of the structural internal effort of the reinforced concrete shallow foundation such as bending moment, axial and shear forces in the HSM is usually larger than that of the MC model. This is due to the difference in the nature of the strain hardening behavior of the HSM.

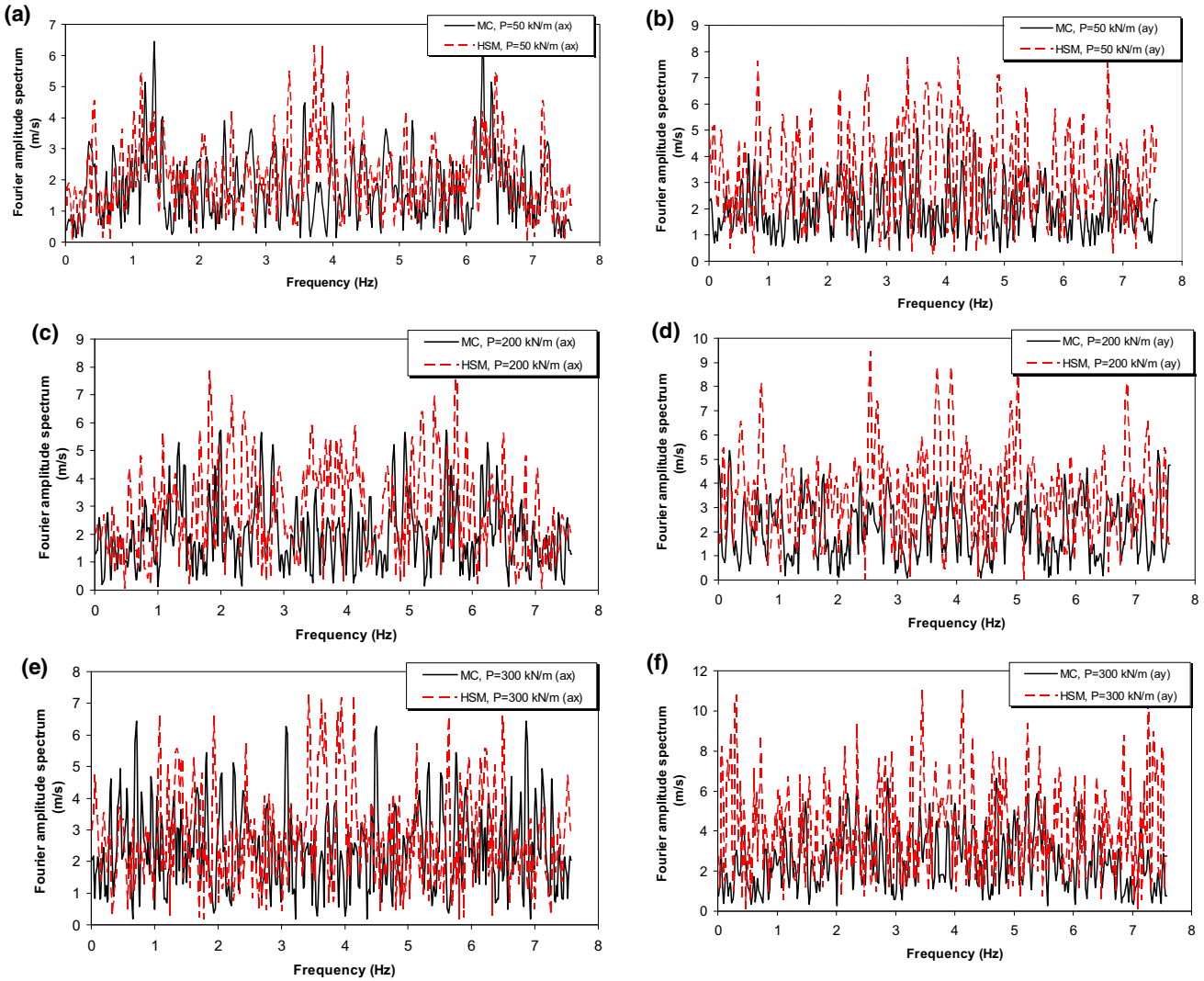

Fig. 20 Fourier amplitude response spectra for horizontal (**a**, **c**, **d**) and vertical (**b**, **d**, **f**) acceleration responses due to different surcharge loads including P = 50, 200 and 300 kN/m

4- The responses of the horizontal and vertical deformations and shear strain of the HSM model are *usually larger* than that of the MC model. This is due to the presence of plastic strains within the hardening zone of the stress–strain elastic–plastic behavior of the HSM model.

5- The horizontal and vertical acceleration responses of the HSM model at most moments of seismic loading *are greater than the MC model*. In fact, the overall pattern of seismic behavior of the acceleration response of the HSM and MC models is similar to their seismic responses in terms of seismic displacements and shear strains. The responses of the both time and frequency domains of the acceleration outputs of the HSM model are larger than the responses of the MC model.

6- The HSM hardening soil model looks more conservative and better, because it produces larger deformations and seismic responses than the MC model. The larger responses of the HSM model are evident in the studied parameters of acceleration, strain, internal effort of the shallow foundation, and slope/footing displacements in most cases. Therefore, the MC model responses are less conservative than the HSM model, although it may provide a more efficient engineering design. Given that the HSM model provides larger structural and geotechnical responses in most cases compared to the MC model for the problem of slope and shallow foundation seismic loading, it seems that this model is more compatible with the reality of the problem and use it as a priority in numerical modeling over the MC model.

7- The basic topic of this paper was the use of non-linear time-history dynamic analyses along with constitutive model changes and surcharge load parametric condition variations, which have been nearly discussed in previous studies. Usually, previous studies have used the *pseudo-*

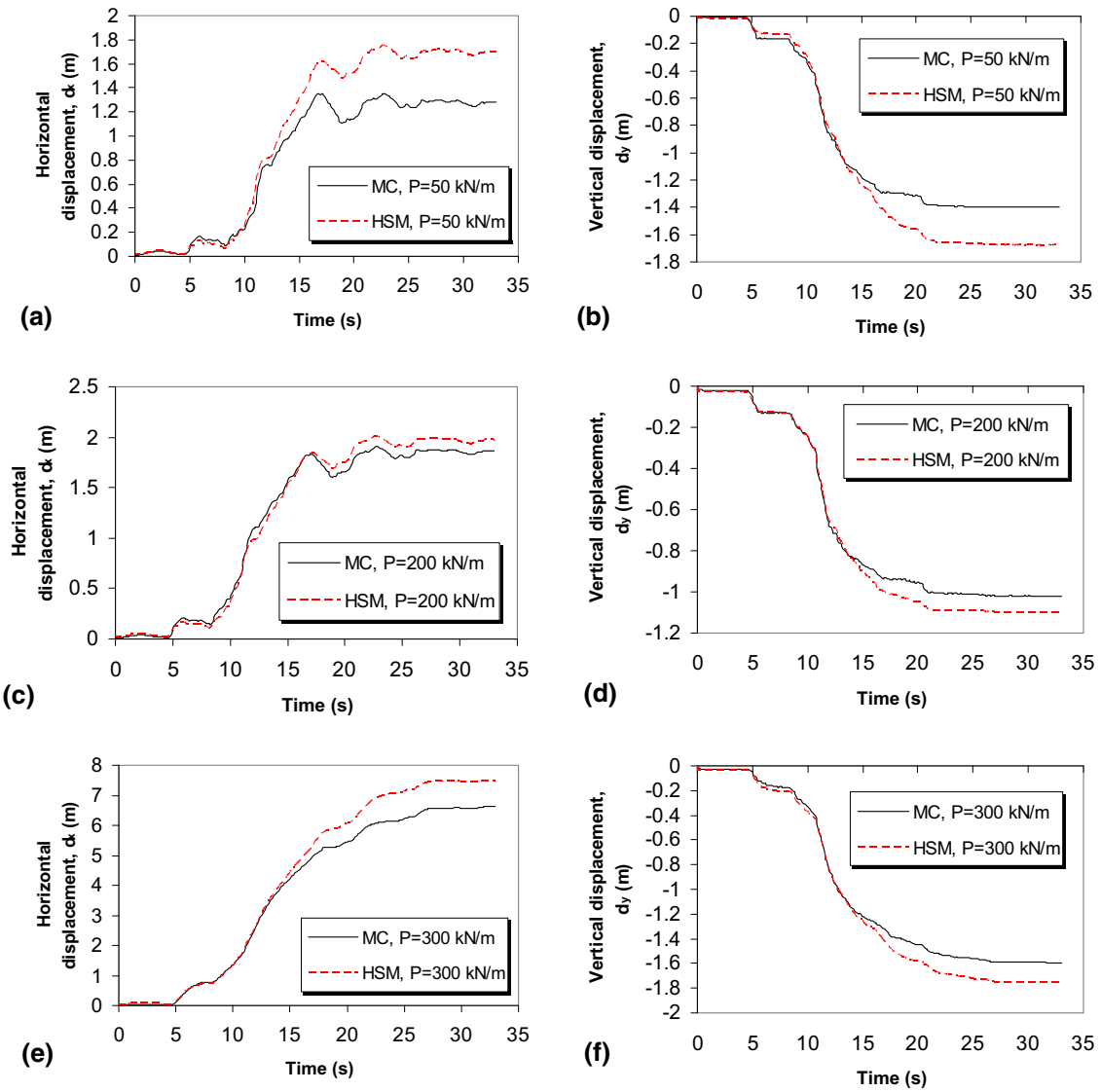

Horizontal displacement reponses of the slope crest

Vertical displacement reponses of the slope crest

Fig. 21 Comparison of the horizontal and vertical displacement responses of the slope in the two MC and HSM models for different surcharge loads (for d = 0.5b case)

static analysis to solve this problem, While, this paper used the real non-linear time-history analyses. The practical application of this research is that engineers and researchers calculate and compare the differences in the response of constitutive models in both structural and geotechnical domains for a real seismic slope-footing model. It should also be noted that actual seismic loading must necessarily include the time and frequency changes of a given earthquake record.

Acknowledgments There is no acknowledgement information for this article. (It is not applicable).

Funding No funding has been provided by the organization for this research.

Declarations

Conflict of interest On behalf of all authors, the corresponding author states that there is no conflict of interest.

References

1. Castelli F, Lentini V (2012) Evaluation of the bearing capacity of footings on slopes. Int J Phys Model Geotech 12(3):112–118
2. Askari F, Farzaneh O (2003) Upper-bound solution for seismic bearing capacity of shallow foundations near slopes. Geotechnique 53(8):697–702
3. Castelli F, Motta E (2010) Bearing capacity of strip footings near slopes. Geotech Geol Eng 28(2):187–198

4. Ausilio E (2014) Seismic bearing capacity of strip footings located close to the crest of geosynthetic reinforced soil structures. Geotech Geol Eng 32(4):885–899
5. Bowles JE (1996) Foundation analysis and design,5th Ed., McGraw-Hill, New York. https://www.amazon.com/Joseph-Bowles-Foundation-1995-09-16-Hardcover/dp/B0146V1T8U
6. Budhu M, Al-Karni A (1993) Seismic bearing capacity of soils. Geotechnique 43(1):181–187
7. Choudhury D, Subba Rao KS (2006) Seismic bearing capacity of shallow strip footings embedded in slope. Int J Geomech 6(3):176–184. https://doi.org/10.1061/(ASCE)1532-3641(2006)6:3(176)
8. Dormieux L, Pecker A (1995) Seismic bearing capacity of foundations on cohesionless soil. J Geotech Eng 121(3):300–303
9. Kumar J, Kumar N (2003) Seismic bearing capacity of rough footings on slopes using limit equilibrium. Geotechnique 53(3):363–369
10. Kumar J, Rao VBKM (2002) Seismic bearing capacity factors for spread foundations. Geotechnique 52(2):79–88
11. Kumar J, Rao VBKM (2003) Seismic bearing capacity of foundations on slopes. Geotechnique 53(3):347–361
12. Paolucci R, Pecker A (1997) Seismic bearing capacity of shallow strip foundations on dry soils. Soils Found 37(3):95–105
13. Richards R, Elms DG, Budhu M (1993) Seismic bearing capacity and settlements of foundations. J Geotech Eng 119(4):662–674
14. Sarma SK (1999) Seismic bearing capacity of shallow strip footings adjacent to a slope. Proc., 2nd Int.Conf. Earthquake Geotechnical Engineering, Lisbon, Portugal, Balkema, Rotterdam, The Netherlands, 309–313. https://doi.org/10.13140/2.1.1749.0880
15. Sarma SK, Iossifelis IS (1990) Seismic bearing capacity factors of shallow strip footings. Geotechnique 40(2):265–273
16. Sawada T, Nomachi SG, Chen WF (1994) Seismic bearing capacity of a mounded foundation near a downhill slope by pseudostatic analysis. Soils Found 34(1):11–17
17. Soubra AH (1997) Seismic bearing capacity of shallow strip footings in seismic conditions. Proc Inst Civ Eng Geotech Eng 125(4):230–241
18. Hansen JB (1970) A revised and extended formula for bearing capacity. Geoteknisk Inst Bull 28:5–11. http://materias.fi.uba.ar/6408/Brinch%20Hansen%20-%20An%20extended%20formula%20for%20bearing%20capacity.pdf
19. Kumar J (2003) Nγ for rough strip footing using the method of characteristics. Can Geotech J 40(3):669–674. https://doi.org/10.1139/T03-009
20. Morrison EE Jr, Ebeling RM (1995) Limit equilibrium computation of dynamic passive earth pressure. Can Geotech J 32:481–487
21. Richards R, Elms DG, Budhu M (1990) Dynamic fluidization of soils. J Geotech Eng 116(5):740–759
22. Saran S, Sud VK, Handa SC (1989) Bearing capacity of footings adjacent to slopes. J Geotech Eng 115(4):553–573
23. Meyerhof GG (1957) The Ultimate Bearing Capacity of Foundations on Slopes. 4th International Conference on Soil Mechanics and Foundation Engineering, 3, 384–386. https://www.scirp.org/(S(351jmbntvnsjt1aadkposzje))/reference/ReferencesPapers.aspx?ReferenceID=1719568. https://nrc-publications.canada.ca/eng/view/ft/?id=f2cc306d-2bab-4592-9817-c9a4f6053b85
24. Meyerhof GG (1963) Some recent research on the bearing capacity of foundations. Can Geotech J 1(1):16–26
25. Soubra AH (1999) Upper bound solutions for bearing capacity of foundations. J Geotech Geoenviron Eng 125(1):59–68
26. Subba Rao KS, Choudhury D (2005) Seismic passive earth pressures in soils. J Geotech Geoenviron Eng 131(1):131–135
27. Vesic AS (1973) Analysis of ultimate loads of shallow foundations. J Soil Mech Found Div 99(1):45–73
28. Zhu DY (2000) The least upper-bound solutions for bearing capacity factor Nγ. Soils Found 40(1):123–129
29. Sharafi H, Shams Maleki Y (2014) p-y curves inc-φ soils by considering pile-soil interface properties effects. The Electronic Journal of Geotechnical Engineering (EJGE), ISSN: 1089–3032; 19(D), 955–970. http://www.ejge.com/2014/Ppr2014.085mar.pdfX
30. Sharafi H, Shams Maleki Y, Karimpour Fard M (2016) Three-dimensional finite difference modeling of static soil-pile interactions to calculate p-y curves in pile-supported slopes. Arab J Geosci 9:5 (2016). https://doi.org/10.1007/s12517-015-2051-9
31. Sharafi H, Shams Maleki Y (2020) Studying seismic interaction of piles row-sandy slope under one, two and triaxial loadings: a numerical-experimental approach. European Journal of Environmental and Civil Engineering. Taylor & Francis.24(9), 1277–1301. SN-1964–8189. https://doi.org/10.1080/19648189.2018.1459323
32. Sharafi H, Shams Maleki Y (2019) Evaluation of the lateral displacements of a sandy slope reinforced by a row of floating piles: a numerical-experimental approach. Soil Dyn Earthq Eng 122(2019):148–170. https://doi.org/10.1016/j.soildyn.2019.04.007
33. Sharafi H, Shams Maleki Y (2019) Evaluation of hazardous effects of near-faultearthquakes on earth dams by using EL and TNL numerical methods (case studies: Gheshlagh Oleya and Jamishan dams). Nat Hazards 98:451–484. https://doi.org/10.1007/s11069-019-03702-4
34. Wu G, Zhao H, Zhao M, Xiao Y (2020) Undrained seismic bearing capacity of strip footings lying on two-layered Slopes, Computers and Geotechnics 122(2020):103539. https://doi.org/10.1016/j.compgeo.2020.103539
35. Zhang R, Xiao Y, Zhao M (2020) Jiang J (2020) Seismic bearing capacity of strip footings placed near c-φ soil slopes. Soil Dyn Earthq Eng 136:106221. https://doi.org/10.1016/j.soildyn.2020.106221
36. Keshavarz A, Beygi M, Vali R (2019) Undrained seismic bearing capacity of strip footing placed on homogeneous and heterogeneous soil slopes by finite element limit analysis. Comput Geotech 113(2019):103094. https://doi.org/10.1016/j.compgeo.2019.103094
37. Ausilio E, Zimmaro P (2015) Displacement-based seismic design of a shallow strip footing positioned near the edge of a rock slope. Int J Rock Mech Min Sci 76(2015):68–77. https://doi.org/10.1016/j.ijrmms.2015.02.010
38. Cascone E, Casablanca O (2016) Static and seismic bearing capacity of shallow strip footings. Soil Dyn Earthq Eng 84(2016):204–223. https://doi.org/10.1016/j.soildyn.2016.02.010
39. Cinicioglu O, Erkli A (2018) Seismic bearing capacity of surficial foundations on sloping cohesive ground. Soil Dyn Earthq Eng 111(2018):53–64. https://doi.org/10.1016/j.soildyn.2018.04.027
40. Barrios G, Larkin T, Chouw N (2020) Influence of shallow footings on the dynamic response of saturated sand with low confining pressure. Soil Dyn Earthq Eng 128(2020):105872. https://doi.org/10.1016/j.soildyn.2019.105872
41. Johari A, Hosseini SM, Keshavarz A (2017) Reliability analysis of seismic bearing capacity of strip footing by stochastic slip lines method. Comput Geotech 91(2017):203–217. https://doi.org/10.1016/j.compgeo.2017.07.019
42. Jafarian Y, Lashgari A (2016) Simplified procedure for coupled seismic sliding movement of slopes using displacement-based critical acceleration. Int J Geomech 16(4):04015101. https://doi.org/10.1061/(asce)gm.1943-5622.0000578
43. Baziar MH, Rezaeipour H, Jafarian Y (2012) Decoupled solution for seismic permanent displacement of earth slopes using

deformation-dependent yield acceleration. J Earthq Eng 16(7):917–936. https://doi.org/10.1080/13632469.2012.689119
44. Lashgari A, Jafarian Y, Haddad A (2018) Predictive model for seismic sliding displacement of slopes based on a coupled stick-slip-rotation approach. Eng Geol 244:25–40. https://doi.org/10.1016/j.enggeo.2018.07.017
45. Lashgari A, Jafarian Y, Haddad A (2020) A coupled stick-slip-rotation model for earthquake-induced sliding displacement of slopes in Iran. Soil Dyn Earthq Eng 135:106199. https://doi.org/10.1016/j.soildyn.2020.106199